Distinct Effect of the Warming Trend on Extreme Mei-Yu Rainfall in June and July over East Asia: Perspectives from Observation and Simulation

AN-YI HUANG,[a,b] CHI-CHERNG HONG,[a] CHAO-AN CHEN,[c] HUANG-HSIUNG HSU,[d] WAN-LING TSENG,[e] PEI-CHUN HSU,[f] MIN-HUI LO,[g] AND JUN CHIANG[a]

[a] *Department of Earth and Life Science, University of Taipei, Taipei, Taiwan*
[b] *College of Earth, Ocean, and Atmospheric Sciences, Oregon State University, Corvallis, Oregon*
[c] *National Science and Technology Center for Disaster Reduction, New Taipei, Taiwan*
[d] *Anthropogenic Climate Change Center, Research Center for Environmental Changes, Academia Sinica, Taipei, Taiwan*
[e] *International Degree Program in Climate Change and Sustainable Development, National Taiwan University, Taipei, Taiwan*
[f] *Academy of Circular Economy, National Chung Hsing University, Taichung, Taiwan*
[g] *Department of Atmospheric Sciences, National Taiwan University, Taipei, Taiwan*

(Manuscript received 15 June 2024, in final form 18 September 2024, accepted 2 December 2024)

ABSTRACT: The record mei-yu rainfall occurred in the Yangtze–Huai River valley (YHRV) and Japan regions in the early summer (June–July) of 2020 and devastated these regions. Whereas several studies had been devoted to the physical processes behind this climate extreme, the impact of the upward trend in the ocean and atmosphere was less investigated. In this study, the potential effect of the linear trend on the mei-yu rainfall extreme was assessed by comparing the 2020 event with a 1998 extreme event. The distinction between June and July was the focus. In June, a significant increasing rainfall trend, accompanied by an enhanced low-level southwesterly, was identified over south China. The linear trend of precipitation also contributed substantially to the total mei-yu rainfall in 2020, which was not observed in 1998. The moisture flux budget indicates that the climatological moisture transport by the linear trend of southwesterly contributes substantially to the extreme rainfall. In contrast to June, the mei-yu rainfall in July over YHRV, accompanied by a low-level easterly trend, showed a decreasing trend. Consequently, the linear trend does not contribute to the extreme rainfall. The numerical experiments, consistent with observations, indicated that the sea surface temperature (SST) warming trend contributed to the extreme mei-yu rainfall in June. This effect was not observed in July.

KEYWORDS: Atmosphere; Atmosphere-ocean interaction; Atmospheric circulation; Large-scale motions; Extreme events; Trends

1. Introduction

The mei-yu front (MYF) is a special feature of the East Asian summer monsoon, and it accounts for 50%–70% of the rainfall in East Asia. The MYF is characterized by a southwest–northeast rain belt and usually migrates from south China and Taiwan to northeast China, the Korean Peninsula, and Japan in early summer (Tao and Chen 1987; Qian and Lee 2000; Wang and LinHo 2002). Studies have indicated that the precipitation induced by the mei-yu rain belt exhibits variability on multiple timescales (e.g., intraseasonal, interannual, and interdecadal fluctuations) and that it is often associated with large-scale atmospheric and oceanic conditions (Weng et al. 1999; Chang et al. 2000a,b; Wu and Wang 2000; Ding et al. 2008; Song et al. 2016; Ding et al. 2020; Wu et al. 2020).

From June to July (i.e., early summer) of 2020, the Yangtze–Huai River valley and Japan (YHRV–Japan) region experienced extreme mei-yu rainfall. The daily accumulated precipitation from 1 May to 1 September 2020 reached a record high of more than two standard deviations (Fig. 1) away from the mean in 1979–2020. The extreme mei-yu rainfall in the YHRV–Japan region caused more than 300 deaths and considerable socioeconomic losses (Wei et al. 2020). During the extreme event, a westward-extending, enhanced western North Pacific subtropical high (WNPSH) was identified; the WNPSH associated anomalous southwesterly winds transported considerable moisture to the MYF and therefore contributed to the 2020 extreme rainfall (Zhao et al. 2021).

Studies have revealed that the interannual variation of the WNPSH is associated with the tropical sea surface temperature (SST) in various basins (Wang et al. 2000; Yang et al. 2007; Xie et al. 2009; Wu et al. 2010; Hong et al. 2014, 2015; Stuecker et al. 2015). Takaya et al. (2020) and Zhou et al. (2021) reported that a high SST in the Indian Ocean (IO) during the early summer of 2020, which followed a record Indian Ocean dipole (IOD) in autumn 2019, contributed substantially to the strong WNPSH through the Indo-western Pacific Ocean capacitor mechanism (Xie et al. 2009). The SST in the North Atlantic was also suggested to have contributed partially to the strong WNPSH in 2020 (Zheng and Wang 2021). However, research indicated that the tropical Pacific SST did not substantially enhance the WNPSH in 2020 (Zhang et al. 2021). In addition to oceanic influences, midlatitude atmospheric perturbations have been reported to have contributed to the heavy mei-yu rainfall; these perturbations include atmospheric blocking in Eurasia (Ding et al. 2021), North Atlantic Oscillation–associated circulation (Liu et al. 2020), and wave trains emigrating from the North Atlantic (Zheng and Wang 2021).

Corresponding author: Chi-Cherng Hong, cchong@utaipei.edu.tw

DOI: 10.1175/JCLI-D-24-0339.1

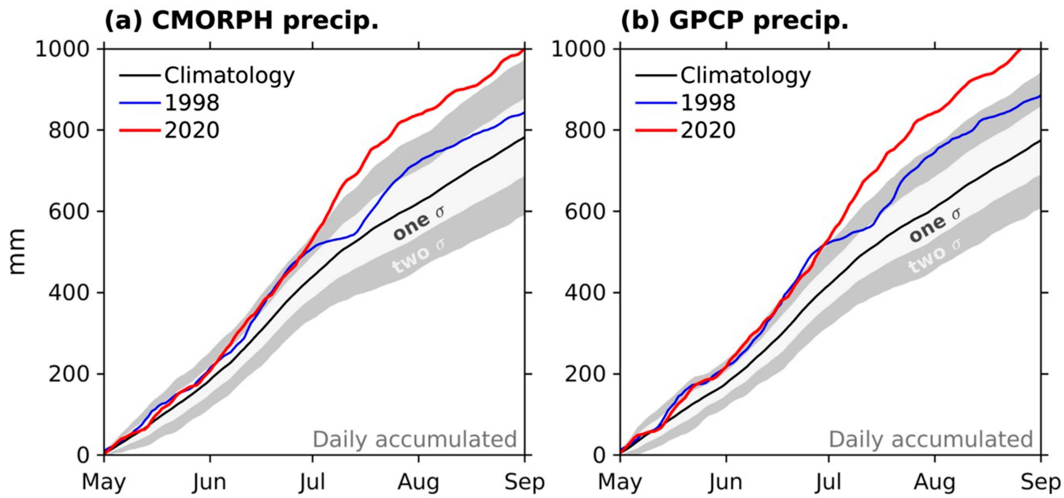

FIG. 1. (a) CMORPH daily accumulated rainfall (mm) from 1 May to 1 Sep in the YHRV–Japan region (MYF: 25°–35°N, 104°–136°E). The black lines are the climatological mean. The blue and red lines are the cases of the year 1998 and 2020, respectively. The light and dark gray shaded regions represent one and two standard deviations σ during 1998–2020, respectively. (b) As in (a), but for GPCP version 1.3.

The SSTs in the tropical IO and western Pacific (i.e., Indo-Pacific) have been exhibiting significant warming trends since the 1950s, and this has contributed substantially to warm pool expansion (Weller et al. 2016). An interesting topic arises: whether these warming trends contributed to the record mei-yu rainfall in the YHRV–Japan region. Additionally, as the mei-yu front migrates northward in response to the annual cycle, the possible effect of SST warming trend on the mei-yu rainfall might differ month by month. Through a literature review, we noted that few studies have thoroughly explored this topic. To investigate the possible effect of the warming trend on the 2020 extreme mei-yu rainfall, we compared the 2020 event with the earlier extreme event (i.e., the second-highest recorded amount of mei-yu rainfall) in 1998, when the Indo-Pacific (IP) warming was not evident. The remainder of this paper is structured as follows: Section 2 presents the data and methods. Section 3 compares the large-scale oceanic and atmospheric conditions of the 1998 and 2020 events. Sections 4 and 5 assess the effect of the warming trend through observational analyses and simulations. In the simulations, we compared the experimental results pertaining to the present and future conditions under a global warming trend.

2. Data and methods

a. Observed data and outputs from climate models

For our observational analysis, we used daily (version 1.3; Huffman et al. 2001) and monthly (version 2.3; Adler et al. 2018) precipitation data from the Global Precipitation Climatology Project (GPCP), satellite daily precipitation data obtained through the Climate Prediction Center morphing technique (CMORPH; Xie et al. 2017), data from the daily Precipitation Estimation from Remotely Sensed Information using Artificial Neural Networks (PERSIANN) precipitation climate data record (Ashouri et al. 2015), and monthly atmospheric data that were obtained from the fifth major global reanalysis produced by the European Centre for Medium-Range Weather Forecasts (ERA5) (Hersbach et al. 2020). We also used monthly oceanic data from version 5 of the Extended Reconstructed sea surface temperature (ERSST) dataset (Huang et al. 2017). The time ranges for the daily and monthly data were 1998–2020 and 1979–2020, respectively.

For the simulations, Atmospheric Model Intercomparison Project (AMIP)-type experiments were conducted using TaiCAM, which is a moderate-resolution atmospheric general circulation model (AGCM) in TaiESM1 (Lee et al. 2020; Wang et al. 2021). The experimental design was described in detail by Kusunoki et al. (2011).

b. Methodology

A percentile rank is the percentage of scores in a reference group that are lower than a given score of interest. Percentiles are expressed as whole numbers between 1 and 99. We used percentiles to evaluate the intensity of the environmental variables in historical records. We also employed correlation coefficients and simple linear regression. For the statistical test, we applied the Student's t test (Student 1908) to determine the significance of the correlation and regression coefficients to verify the presence or absence of a monotonic trend for the interest variables (e.g., precipitation). We calculated moisture flux (defined as the product of specific humidity and horizontal winds) to measure water vapor transport.

3. Comparison of extreme mei-yu rainfall in 1998 and 2020

a. Precipitation and associated large-scale circulation

Figure 1 presents a comparison of the accumulated rainfall in the YHRV–Japan region (25°–35°N, 104°–136°E) from

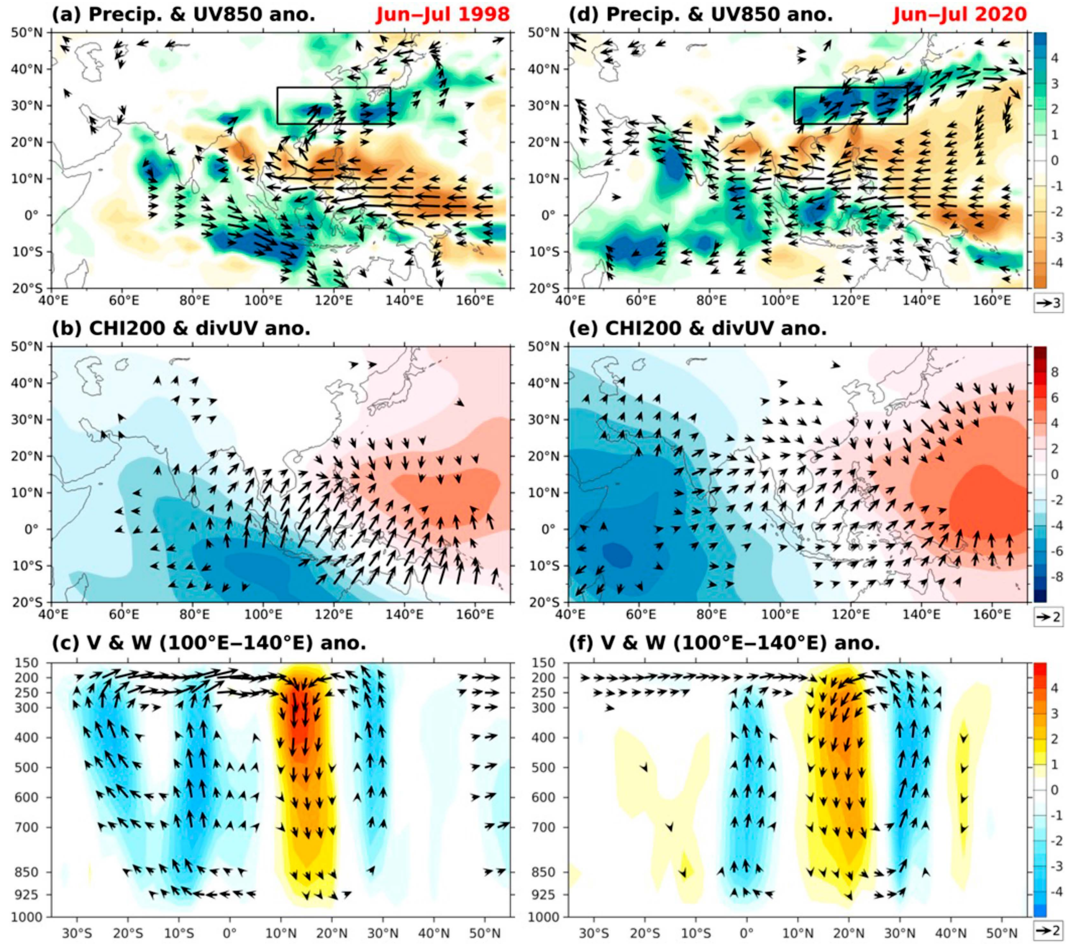

FIG. 2. The 1998 June–July averaged anomalous (a) precipitation (shading; mm·day^{-1}) and horizontal winds at 850 hPa (vectors; m·s^{-1}; minimum vector: 1.5), (b) velocity potential (shading; 10^6 m^2·s^{-1}) and divergent winds at 200 hPa (vectors; m·s^{-1}; minimum vector: 1), and (c) vertical velocity (*w*; shading; 10^{-2} Pa·s^{-1}) and meridional wind (v; vectors are v and *w*; m·s^{-1} 10^{-3} Pa·s^{-1}; minimum vector: 1) averaged over 100°–140°E. (d)–(f) As in (a)–(c), respectively, but for 2020. The black boxes in (a) and (d) depict the region for the MYF index.

1 May to 1 September in 1998 and 2020. The climatological accumulated rainfall from 1 May to 1 August was approximately 620 mm. It approached 720 mm in 1998 and 840 mm in 2020 (Fig. 1a). The accumulated rainfall in 2020 was more than two standard deviations σ away from the climatological mean (1998–2020) and was the highest amount of rainfall in the area during the aforementioned months since 1998. Figure 1 reveals that a rapid increase (from 208 to 705 mm) in accumulated rainfall occurred from early June to mid-July, which was concurrent with extreme rainfall in the region. The time series of the accumulated rainfall from the GPCP dataset (Fig. 1b) displays consistent results with that of the CMORPH rainfall estimates (Fig. 1a), indicating that the record rainfall in 2020 was robust. Figure 1 also indicates that 2020 was a long-duration and persistent mei-yu event. By contrast, the 1998 event experienced double mei-yu rainfalls, with a break during late July to early August.

Figure 2 presents a comparison of the two extremes associated with large-scale circulation and precipitation. From June to July, a zonally distributed positive precipitation anomaly in the YHRV–Japan region (i.e., the MYF) and an anomalous low-level anticyclone in the WNP were clearly identified in both 1998 and 2020 (Figs. 2a,d, respectively). A meridional tripole (wet–dry–wet) rainfall pattern, which was similar to the leading empirical orthogonal function (EOF) of precipitation in early summer (Wang et al. 2008), was observed in East Asia. This pattern resembles the negative phase of the Pacific–Japan teleconnection pattern (Nitta 1987; Kosaka and Nakamura 2006) and has been proposed to be a main driver of the extreme mei-yu rainfall in 2020 (Ding et al. 2021). Despite this similarity, these two extremes have several differences.

First, relative to the WNPSH in 1998, the WNPSH in 2020 was stronger and exhibited a northward and westward extension (Figs. 2a,d). The westward extension of the WNPSH in 2020 caused the low-level easterly anomaly to extend westward to the north IO (NIO); this phenomenon was not identified in the 1998 event. A stronger WNPSH created a stronger southwesterly moisture flux in its western flank in situ and

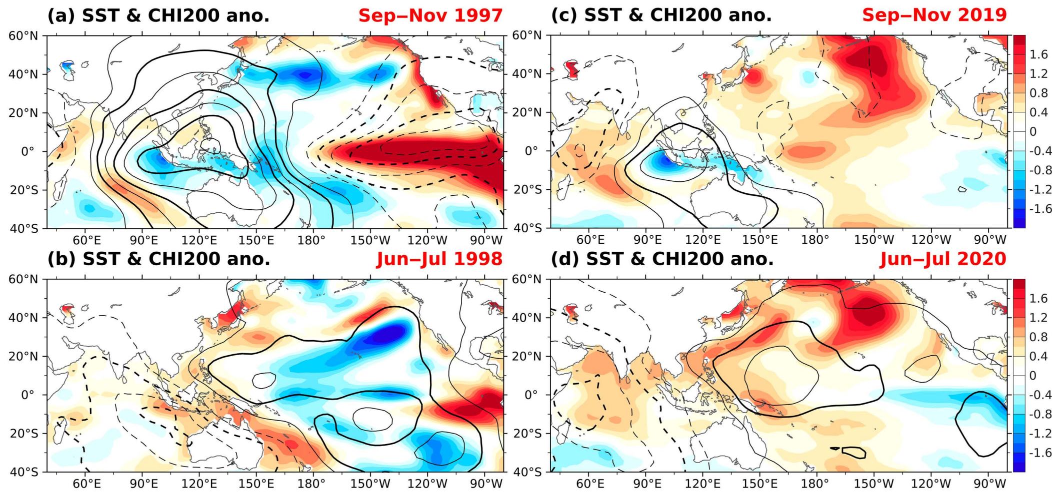

FIG. 3. (a) Anomalous SST (shading; °C) and velocity potential at 200 hPa (CHI200; contour; 10^{-6} $m^2 \cdot s^{-1}$) in September–November 1997. (b) As in (a), but in June–July 1998. (c) As in (a), but for 2019. (d) As in (b), but for 2020.

transported more warm water vapor to the YHRV–Japan region (Zheng and Wang 2021).

Second, the upper-level (200 hPa) velocity potential (CHI200) anomaly that occurred in 1998 exhibited a southwest–northeast distributed structure with ascending and descending centers in the tropical southeastern IO and WNP, respectively (Fig. 2b). By contrast, the CHI200 anomaly in 2020 yielded a zonally distributed dipole with ascending and descending centers in the tropical western–central IO and WNP, respectively (Fig. 2e). Unlike the 1998 event, the westward shift of the ascending center in the 2020 event was associated with a high SST in the central–western IO (Figs. 3b,d). The meridional vertical circulation over East Asia (averaged over 100°–140°E) also exhibited a substantially different structure between 1998 and 2020 (Figs. 2c,f). The ascending branch in the tropics was centered near 10°S in 1998 but moved northward to the equator in 2020 (i.e., over the Maritime Continent). The northward ascending center modified the descending branch in the WNP to expand northward to 25°N in 2020 compared with 1998. The overturning circulation in the WNP–YHRV region in 2020 was also slightly stronger than that in 1998 (Figs. 2c,f); that is, the anomalous ascent in the YHRV–Japan region in 2020 was larger than that in 1998. Notably, an anomalous diabatic heating (ascent) in the Maritime Continent was identified in the 2020 event, and it contributed to the enhancement of the local Hadley circulation and the WNPSH. This effect, which is similar to those reported by other studies (Lu 2001; Sui et al. 2007), was not observed in the 1998 event.

b. *Tropical SSTs*

Studies have reported tropical SSTs to have effects on the WNPSH (Wang et al. 2000; Xie et al. 2009; Hong et al. 2014), which plays a crucial role in determining the intensity and location of MYF rainfall. Researchers have suggested that the strength of a WNPSH can be enhanced by the eastern Pacific–type El Niño in the subsequent summer because of the local air–sea interaction in the WNP (Wang et al. 2000). The 1998 event was preceded by a strong eastern Pacific–type El Niño (Fig. 3a). In addition, notable positive and negative SST anomalies were respectively identified in the western and eastern WNP during the subsequent summer (Fig. 3b), indicating that the local air–sea interaction contributed substantially to the enhancement of the WNPSH. However, the 2020 event was preceded by a weak central Pacific–type El Niño event (Fig. 3c), and no east–west dipole SST anomaly pattern was observed in the WNP (Fig. 3d). No clear evidence suggests that the enhanced WNPSH in 2020 was determined by the SST anomaly in the tropical Pacific (Zhang et al. 2021).

A notable warming in the Indo-Pacific (Fig. 3d) during the boreal early summer in 2020 was observed. This basin warming was not observed for the 1998 event (Fig. 3b). The warming in IO substantially modulated the strength of the Asian summer monsoon (Xie et al. 2009; Hong et al. 2015; Chang et al. 2016). It was reported to be the major factor that contributed to the enhancement and westward extension of the WNPSH in 2020 (Takaya et al. 2020; Zhou et al. 2021).

The time series of mei-yu rainfall–associated large-scale features are presented in Fig. 4. The MYF (Fig. 4a), WNPSH (Fig. 4b), and NIO (Fig. 4c) indices reached record highs during the 2020 event, with the values the highest they had been since 1979. The NIO warming occurred in 1998 and 2020. The high NIO SST in 1998 primarily resulted from the El Niño–associated remote effect, which shifted the climatological state of the Walker circulation (Klein et al. 1999; Webster et al. 1999; Lau and Nath 2003). However, the NIO warming in 2020 occurred for different reasons. Takaya et al. (2020) and Zhou et al. (2021) suggested that a large part of the high NIO SST in 2020 was attributed to the record IOD in 2019 through the oceanic processes. Additionally, the NIO exhibited a clear upward linear trend (0.14°C $decade^{-1}$) from 1979 to 2020 (gray bars in Fig. 4c). This upward trend accounted for more than 40% of the NIO SST anomaly in 2020. By contrast, an effect of the upward trend on the NIO SST in 1998 was not

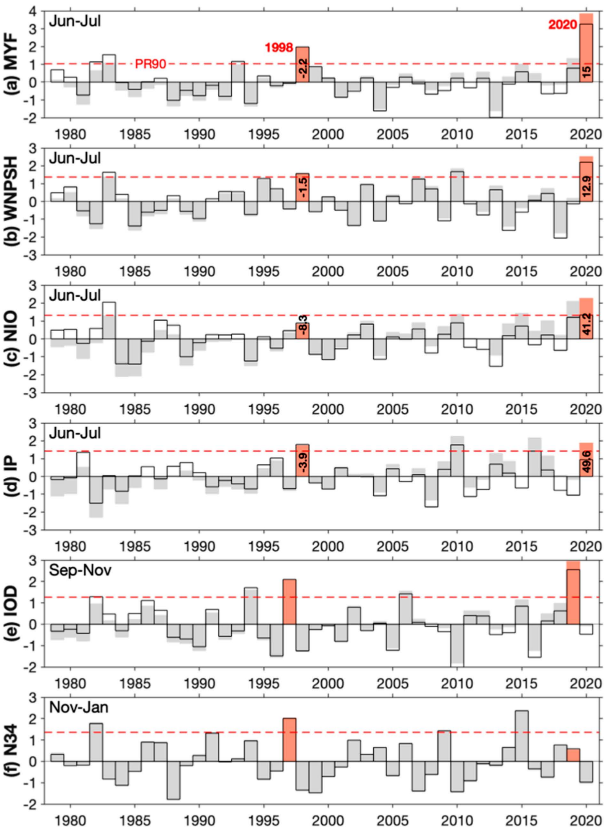

FIG. 4. Normalized anomalies (gray bars) of the (a) June–July averaged MYF index derived from precipitation rate (mm·day^{-1}; 25°–35°N, 104°–136°E), (b) June–July averaged WNPSH index derived from streamfunction at 850 hPa (m^2·s^{-1}; 15°–25°N, 115°–140°E), (c) June–July averaged NIO index derived from SST (°C; 0°–25°N, 40°–100°E), (d) June–July averaged IP index derived from SST (°C; 10°S–10°N, 110°–150°E), (e) September–November averaged IOD index derived from SST (°C) difference between western IO (10°S–10°N, 50°–70°E) and eastern IO (10°S–0°, 90°–110°E), and (f) November–January averaged Niño-3.4 (N34) index derived from SST (°C; 5°S–5°N, 170°E–120°W). The red bars in (a)–(d) and (e) and (f) indicate the year 1998/2020 and 1997/2019, respectively. The outline bars depict the indices after removing the linear trend from 1979 to 2020. The red dash lines represent the 90th percentile (PR90) threshold. The numbers near those red bars are the estimated contribution (%) of the linear trend to the total value.

noted. When the linear trend was re-estimated using a longer period (1959–2020), its contribution to the 2020 event was mostly unchanged, indicating that the upward trend of the high NIO SST in 2020 was robust. The major differences between the 1998 and 2020 events are summarized in Table 1. Although the WNPSH was strong in both 2020 and 1998, these two time periods exhibited several differences with respect to the processes that maintained the unusually strong WNPSH. The role of the warming trend in causing the record NIO SST, which could be a crucial factor, as suggested by Takaya et al. (2020), enabling the enhancement of the WNPSH to be maintained, was notable in 2020. By contrast, the effect of the warming trend was not yet notable in 1998. In addition, El Niño–associated remote forcing, which was not prominent in 2019–20, contributed substantially to the warming NIO SST in 1997–98.

4. Effect of warming trend in SST and humidity on the extreme mei-yu rainfall

a. Analysis based on observations of recent four decades

Figure 5 presents a plot of the linear trends for SST and vertically integrated specific humidity q from 1979 to 2020. An L-shaped warming trend was identified in the tropical western Pacific. The significant warming in the northeastern Pacific (near 40°N, 150°W) was suggested to have a potential effect on the nearby marine heat waves and drought in western America (Liang et al. 2017). The other notable warming trend, which occurred in the midlatitude of the North and South Pacific, was coupled with an upward trend in the mid–upper geopotential height (Figs. 6c,d). Overall, the spatial pattern of the linear trend of q resembled the SST warming trend (pattern correlation coefficient, $r = 0.42$, $p < 0.01$). For example, in the present study, the upward trend of q in the NIO was closely correlated with the warming trend of the SST; the upward trend of q from the northeast of Taiwan to Japan was correlated with the L-shaped SST warming trend in the western Pacific. In addition, we noted that the SST warming trend shown in Fig. 5a might be attributed to natural decadal variability and anthropogenic forcing (Wu et al. 2019).

Because the monsoon circulation and mei-yu rainfall migrate northward in response to the annual cycle, we further investigate the trend of low-level (850 hPa) wind and the associated moisture flux in June and July individually. In June, it reveals that the moisture flux convergence (MFC) over the mei-yu region (located in south China) exhibits a significant increasing trend during 1979–2020. The increase in MFC was primarily induced by an enhanced southwesterly flow and cyclonic circulation anomaly (Fig. 6a). Analysis indicates that the enhanced southwesterly was associated with the increasing trend of 850-hPa streamfunction (SF850) and geopotential height (Z850) in the WNP (Fig. 6c). In July, the trend of MFC does not move northward accompanied by the migration of the mei-yu front (Fig. 6b). It still stayed in south China and even experienced a southward shift compared with June. In contrast to June, the MFC in the mei-yu region (YHRV) yielded a decreasing trend in July. The decreasing trend was associated with a northeasterly trend, which was against the southwesterly monsoon flow (Fig. 6c). It decreased the mei-yu rainfall and led to a slight decreasing rainfall trend in the YHRV. This indicates that the warming trend did not play a critical role in the extreme mei-yu rainfall observed in July 2020. A similar result was reported in earlier studies (Liu et al. 2020; Ding et al. 2021). The northeasterly trend was related to the increasing trend of zonally distributed Z850 (anticyclone like) in the extratropical North Pacific (Fig. 6d). The increasing trend of Z850 exhibits an equivalent barotropic structure, which extends to mid–upper atmosphere and was suggested to have an effect on broadening the coverage of heat waves in

TABLE 1. Comparison of large-scale circulation and background conditions during the extreme mei-yu rainfall events in 1998 and 2020.

Comparison		1997–98	2019–20
YHRV–Japan rainfall (JJ)		Second	First
Associated dominant pattern (JJ; Wang et al. 2008)		EOF1	EOF1
WNPSH (JJ)	Intensity	Third	First
	Location	WNP	WNP with westward and northward expansion
	Maintenance factors	1) Local air–sea interaction (Wang et al. 2000) 2) NIO SST (Xie et al. 2009) 3) MC heating (Sui et al. 2007)	1) NIO SST (Takaya et al. 2020; Zhou et al. 2021) 2) MC heating
SSTA	IOD (SON)	Second (positive)	First (positive)
	Niño-3.4 (NDJ)	Second strong El Niño	Weak El Niño
	NIO (JJ)	Weak (positive)	First (positive)
	WNP (JJ)	West (warm)–east (cold) dipole	Uniform warm
Overturning circulation	Indo-Pacific Ocean interaction (ONDJ)	ENSO–IOD coupling (ascending over eastern Pacific and descending over Indo-western Pacific)	Not obvious
	IO–WNP (JJ)	Southwest–northeast vertical circulation (ascending over east IO and descending over WNP)	Near zonal (west–east) vertical circulation (ascending over west–central IO and descending over WNP)
Trend effect (1979–2020)		Not significant	1) SST in IO and western Pacific (warm pool expansion) 2) Specific humidity in IO, MC, and north Taiwan–southern Japan

the extratropical Northern Hemisphere in recent decades (Hong et al. 2021). The aforementioned clearly demonstrated that the trend of moisture flux in June differs from that in July. This distinction leads the linear trend to have opposite effects on the mei-yu extreme rainfall.

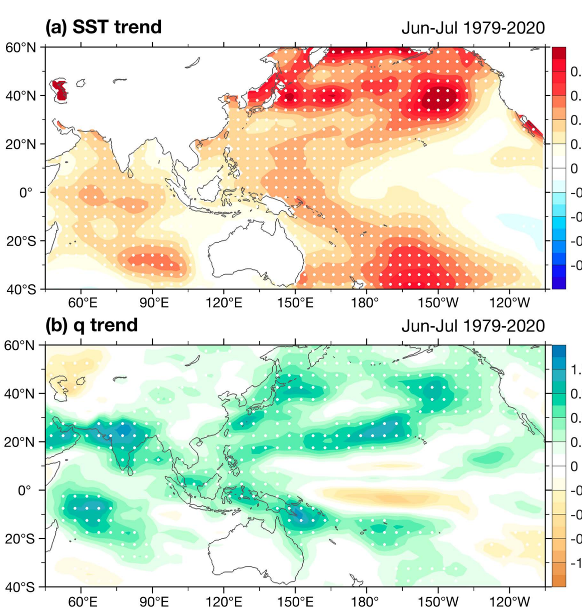

FIG. 5. (a) Linear trend of June–July averaged anomalous SST from 1979 to 2020 (shading; °C yr^{-1}). (b) As in (a), but for vertically integrated (surface to 300 hPa) specific humidity (q; shading; g$\cdot m^{-2}$ yr^{-1}). The stippling indicates the values at each grid are statistically significant (90% confidence level) based on the Student's t test.

b. *Moisture flux budget*

The moisture flux budget was further applied to investigate the potential effect of the warming trend in circulation and specific humidity on the extreme mei-yu rainfall in 2020 and 1998. The moisture flux can be written as

$$\mathrm{U}q = \Big(\underbrace{U_c}_{\text{climatology}} + \underbrace{U_{\mathrm{at}} + U_{\mathrm{ar}}}_{\text{anomaly}}\Big)\Big(\underbrace{q_c}_{\text{climatology}} + \underbrace{q_{\mathrm{at}} + q_{\mathrm{ar}}}_{\text{anomaly}}\Big)$$

$$= \underbrace{U_c q_c}_{\substack{\text{pure}\\ \text{climatology}}} + \underbrace{U_c q_{\mathrm{at}} + U_c q_{\mathrm{ar}}}_{\substack{\text{moist decompose}\\ \text{with wind climatology}}} + \underbrace{U_{\mathrm{at}} q_c + U_{\mathrm{ar}} q_c}_{\substack{\text{wind decompose}\\ \text{with moisture climatology}}}$$

$$+ U_{\mathrm{at}} q_{\mathrm{at}} + U_{\mathrm{at}} q_{\mathrm{ar}} + U_{\mathrm{ar}} q_{\mathrm{at}} + U_{\mathrm{ar}} q_{\mathrm{ar}}, \quad (1)$$

where U represents the horizontal wind, q represents the specific humidity, and Uq represents the horizontal moisture flux. The subscript "c" denotes climatology, while "a" denotes anomaly. The total anomaly was further decomposed into two terms: the trend component "at" and the residual component (i.e., detrending anomaly) "ar". Because the right-hand side in Eq. (1) is dominated by the first five terms, briefly, the following analysis is focused on these terms.

In June 2020, the structure of MFC (shadings in Fig. 7) was dominated by the annual cycle of the term $U_c q_c$ (Fig. 7a). The $U_{\mathrm{at}} q_c$ contributed to the above-normal MFC (Fig. 7f), whereas the terms $U_c q_{\mathrm{ar}}$ and $U_{\mathrm{ar}} q_c$ modified the MFC or mei-yu rain belt to extend northward (Figs. 7e,g). The contribution of residual moisture flux from the wind trend component (Fig. 7f) appears to have a much more southward distribution compared to Fig. 7a. This is because the wind trend in June,

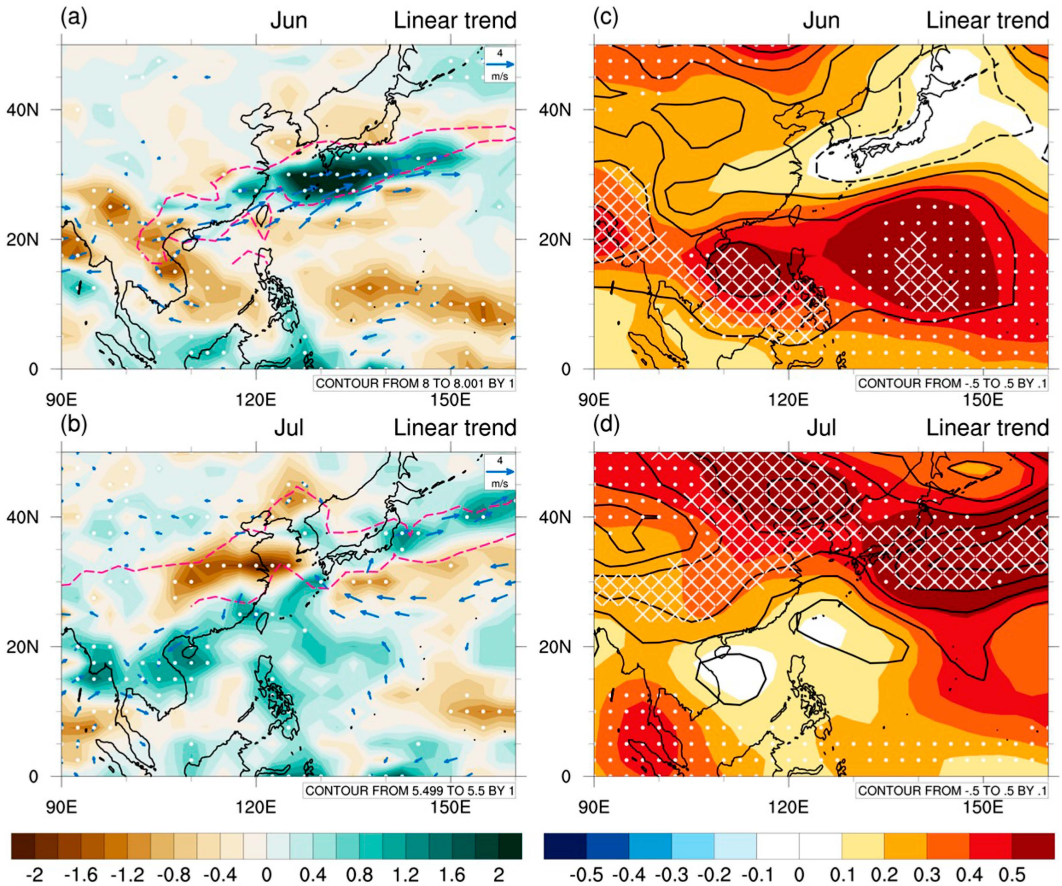

FIG. 6. (a) Linear trend of vertically integrated (from surface to 300 hPa) MFC (shading; $g \cdot m^{-2} \cdot s^{-1} \cdot yr^{-1}$) and horizontal winds (UqVq; vectors; $g \cdot m^{-1} \cdot s^{-1} \cdot yr^{-1}$) in June from 1979 to 2020. The white dots denote the linear trend that exceeds 90% confidence level based on the Student's *t* test. The red dashed contour indicates the 8.0 mm (June) and 5.5 mm (July) of the climatological rainfall. (b) As in (a), but for July. (c) Linear trend of SF850 (shading; $10^5 \cdot m^2 \cdot s^{-1}$) and Z850 (contour; m) in June from 1979 to 2020. The white dots (SF850) and crosses (Z850) denote the linear trend that exceeds 90% confidence level based on the Student's *t* test. (c) As in (d), but for July.

the southwesterly winds (Fig. 6a), was located south of the YHRV. That is, the increase in MFC in the mei-yu region primarily resulted from the climatological specific humidity transport by the linear trend of the southwesterly flow. During July, the major structure of MFC (i.e., mei-yu rainfall) was also dominated by the term $U_c q_c$ (Fig. 7h). In contrast to June, the term $U_{at} q_c$ tends to lead to an MFC decrease in the mei-yu region due to the linear trend of low-level northeasterly winds opposing the southwesterly monsoon flow (Fig. 7m). The increase in MFC primarily resulted from the $U_{ar} q_c$ (Fig. 7n). Here, U_{ar} was associated with the interannual variation of an enhanced southwesterly monsoon flow, which was induced by the anomalously strong WNPSH. Thus, interannual variation rather than the linear trend contributed to the mei-yu rainfall increase in July 2020.

Figure 7, consistent with Fig. 5, reveals that the effect of the linear trend on the mei-yu extreme rainfall was different between June and July. The linear trend accounts for the rainfall increase in June, whereas the interannual variation of WNPSH plays the dominant role in July. The same analysis was applied to 1998 (Fig. 8). It revealed that the mei-yu rainfall increase was caused by the terms $U_{ar} Q_c$ and $U_c Q_{ar}$. No evident contribution of $U_{at} q_c$ to the MFC was identified. In contrast to 2020, the extreme mei-yu rainfall in June and July was determined solely by the interannual variation and the enhanced southwesterly monsoon flow caused by an enhanced WNPSH.

5. Numerical experiments

The observation suggests that the linear trend of MFC contributed considerably to the extreme mei-yu rainfall in June. Figure 5 shows that the trend of rainfall is well correlated with the SST trend. In this section, the AMIP-type experiments by TaiCAM (AGCM in the TaiESM1; Lee et al. 2020; Wang et al. 2021) were conducted to estimate the possible effect of linear trend of SSTs on the extreme mei-yu rainfall. Two experiments were conducted. In the first experiment (referred to as CTR-exp), the model was forced by the observed monthly SST integrated from 1961 to 2020. The second experiment (referred to as Dtrnd-exp) was same as CTR-exp

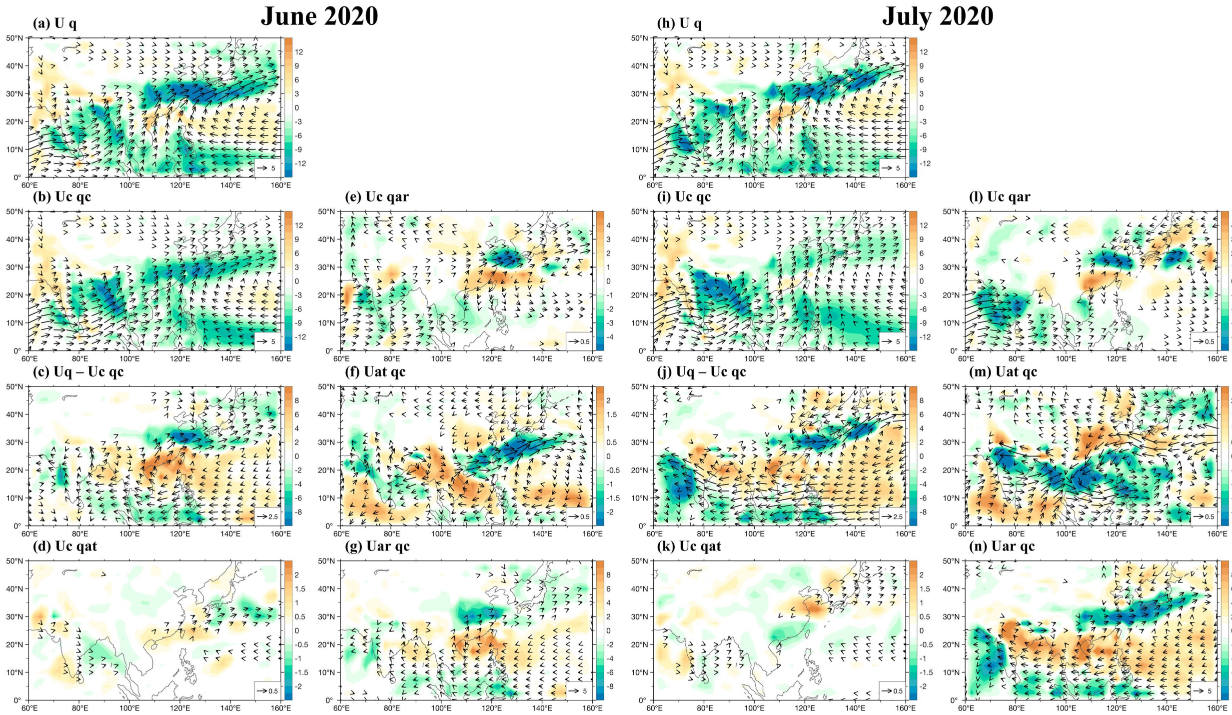

FIG. 7. Decomposition of moisture flux for June and July in 2020. The detail of decomposition was documented in Eq. (1). The shadings represent the vertically integrated (surface to 300 hPa) MFC (10^{-7} kg·m^{-2}·s^{-1}). Vectors indicate the vertically integrated horizontal moisture flux [(m·s^{-1}) (kg·kg^{-1})]. The long-term trend is calculated from 1979 to 2020.

except that the model was forced by the detrended SST; that is, the linear trend was subtracted from the total SST during 1961–2020. The difference between Dtrnd-exp and CTR-exp can be assumed to represent the effect of the linear trend of SST.

The numerical experiments reveal that the distinction of linear trend in rainfall between June and July was realistically duplicated by the TaiCAM (comparing Figs. 6a,b with Figs. 9a,b). That is, the warming trend substantially contributes to mei-yu rainfall in the YHRV in June (Fig. 9c), while conversely, it tends to decrease the mei-yu rainfall in July. Additionally, the increase (decrease) mei-yu rainfall accompanied by southwesterly (northeasterly) in June (July) was also successfully simulated.

The effect of SST trend on the extreme mei-yu rainfall is further estimated by the change rate of rainfall extreme written as

$$\mathrm{CRatio} = \Delta R_x / R_x, \tag{2}$$

where R_x indicates the PR95 of rainfall for each grid in the CTR-exp during 1979–2020, ΔR_x depicts the difference of PR95 between the Dtrnd-exp and CTR-exp, and CRatio indicates the change rate of PR95 induced by the linear SST trend relative to observed SST. Overall, the CRatio exhibits a similar pattern with the change of mean rainfall (Fig. 10). The distribution of CRatio revealed that the linear SST trend tends to enhance the mei-yu rainfall by approximately 10%–20% in June. Conversely, the SST trend decreases the extreme rainfall in the YHRV in July. Notably, the CRatio in Japan differing from the YHRV also revealed an increase in July. The numerical experiments, confirming the observation, indicate that the linear trend of SST has a substantial impact on amplifying the mean and extreme mei-yu rainfall in June. However, the effect of linear SST trend on mei-yu rainfall in July yields contrast feature compared with June. It tends to decrease both mean and extreme mei-yu rainfall in the YHRV.

6. Conclusions and discussion

The YHRV–Japan region experienced extreme mei-yu rainfall in the June and July of 2020, during which time the record amount of mei-yu rainfall had devastating consequences. In the present study, the physical processes that caused the 2020 extreme event were investigated through observation and climate simulation. The potential effect of the SST warming trend on the 2020 extreme event was analyzed by comparing it with an earlier extreme event that occurred in 1998. The main results are summarized as follows:

1) The record mei-yu rainfall in the YHRV–Japan region in 2020 was accompanied by a record WNPSH and Indo-Pacific SST. The monsoon circulation associated with the record WNPSH transported anomalous moisture, contributing substantially to the mei-yu rainfall. The record NIO SST induced overturning circulation in the Indo-western Pacific that played a crucial role in maintaining the record WNPSH.

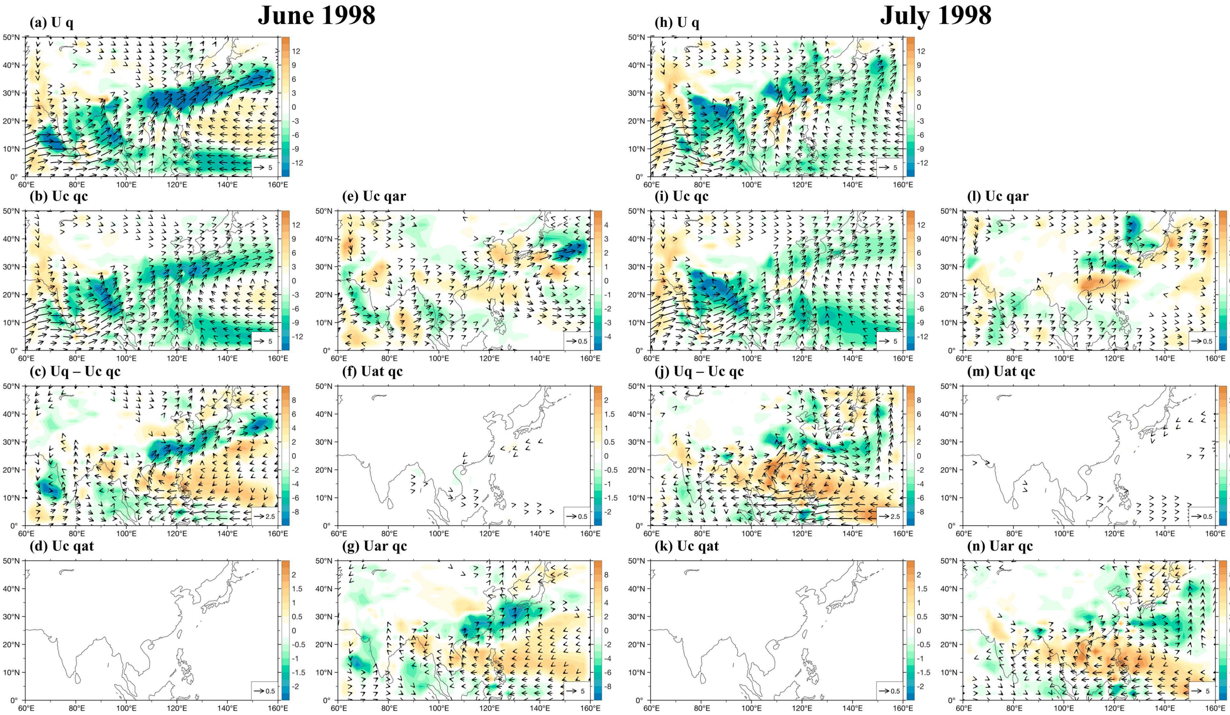

FIG. 8. As in Fig. 7, but for 1998.

2) A significant upward trend in the Indo-Pacific SST was identified. The linear upward trend accounted for approximately 40% of the total SST variation in 2020 but did not have a discernible effect on the 1998 event. In addition to the upward SST trend, a significant upward moisture trend was identified in the mei-yu region from the northeast of Taiwan to Japan. The upward moisture trend was correlated with the upward SST trend and reflected the trend of the MYF index.

3) Observation revealed that the mei-yu rainfall in the YHRV had a different trend between June and July. The rainfall revealed a significant upward linear trend in June during 1979–2020. Conversely, it yielded a weak downward trend in July. This distinction made the linear trend have an opposite contribution to the mei-yu extreme rainfall in 2020. The upward trend accounted for approximately 30% of the total mei-yu rainfall in June, while no evident contribution was identified in July.

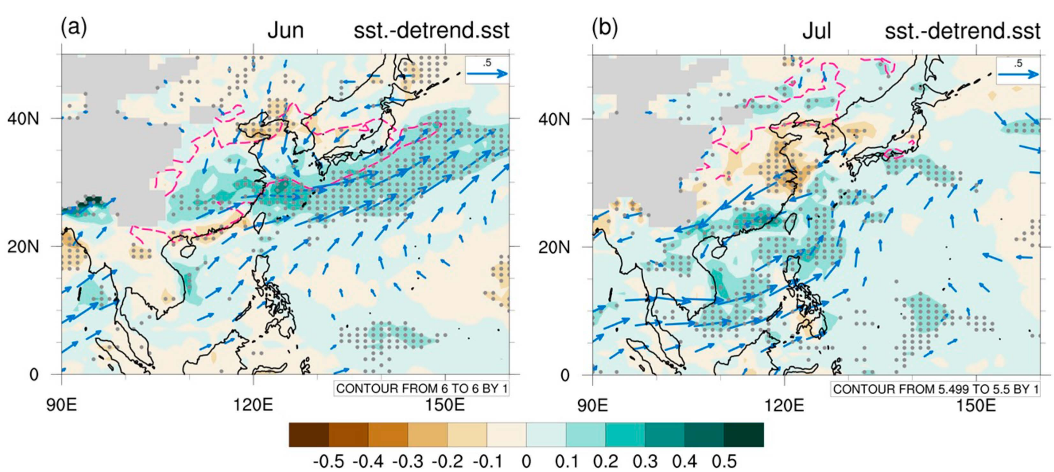

FIG. 9. (a) Difference in vertically integrated (from surface to 300 hPa) MFC (shading; 10^{-1} g·m^{-2}·s^{-1}·yr^{-1}) and horizontal winds (UqVq; vectors; 10^{6} g·m^{-1}·s^{-1}·yr^{-1}) between CTR-exp and Dtrnd-exp in June. (b) As in (a), but for July. The gray polygon is the terrains over 850-hPa pressure level. The red-dashed contour lines in (a) and (b) indicate the 6.0 mm (June) and 5.5 mm (July) of climatological rainfall. The white dots and blue vectors denote the linear trend that exceeds 90% confidence level based on the Student's t test.

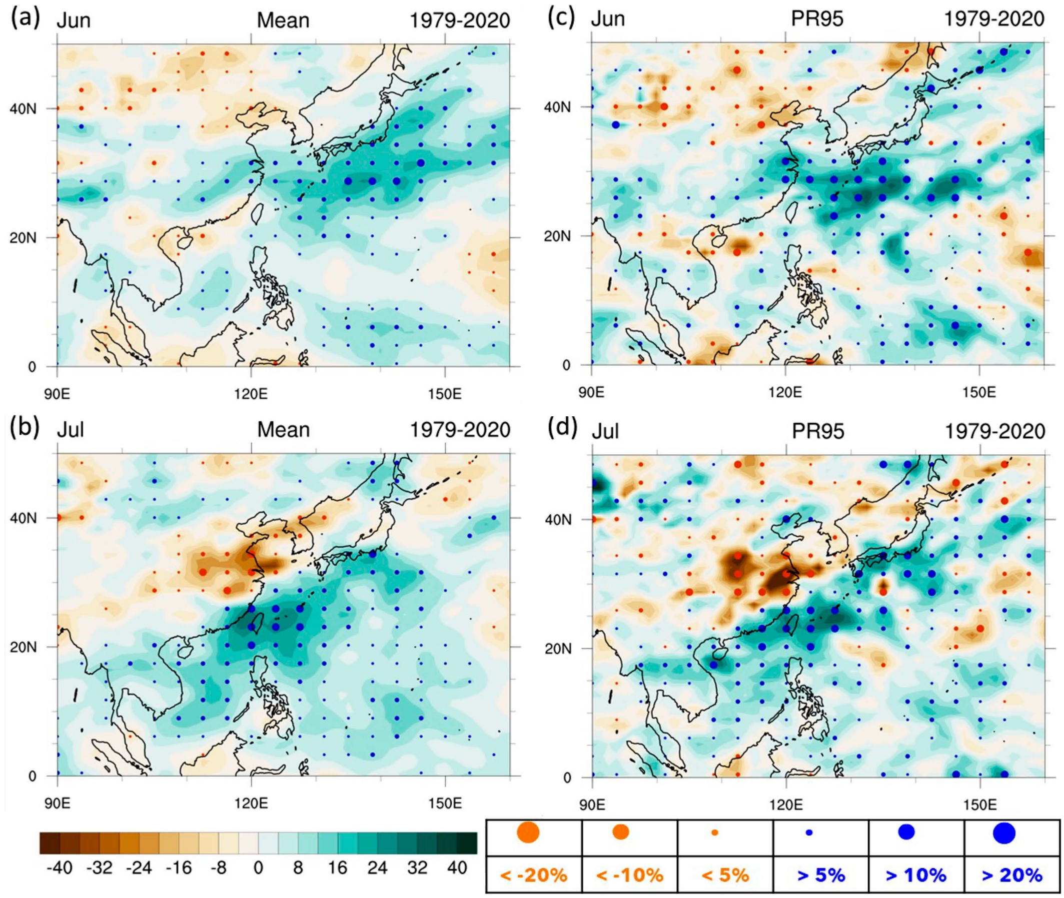

FIG. 10. (a) Difference in climatological (1979–2020) rainfall (shading) in June between CTR-exp and Dtrnd-exp. The blue small, middle, and large dots represent the contribution of SST trend on the mean rainfall larger than 5%–10%, 10%–20%, and >20%, respectively. The orange dots are the same as the blue dots expect that the CRatio is negative. (b) As in (a), but for July. (c),(d) As in (a) and (b), but for the change rate of extreme rainfall (PR95). The definition of CRatio was documented in Eq. (2).

4) The moisture flux budget further indicates that the climatological moisture transport by the linear trend of southwesterly enhances substantially the MFC and mei-yu rainfall in June. Conversely, the MFC over the YHRV, which was accompanied by a low-level easterly, yielded a decreasing trend. Consequently, the linear trend does not have an evident contribution to the extreme rainfall. The distinct effect of the SST warming trend on the mei-yu rainfall between June and July was further confirmed by the numerical experiments from the TaiCAM model. Consistent with observations, the SST warming trend contributed to the extreme mei-yu rainfall extreme in June but it was not observed in July.

Although several studies have reported on the role of the NIO SST in maintaining the unusually strong WNPSH in 2020, few have explored the relative contribution of the warming trend. Our study revealed that the upward trend accounted for approximately 40% of the total anomaly in NIO SST in 2020. We estimate the effect of linear SST trend on mei-yu rainfall by comparing Dtrnd-exp and CTR-exp. The numerical experiments confirming the observation indicate that the linear trend of SST increases substantially the mei-yu mean rainfall and extreme rainfall over the YHRV during June. However, the SST trend in July yields contrast impact compared with June.

The distinctions between June and July were associated with differences in the trend of Z850 (Figs. 6c,d). The upward trend of geopotential height (i.e., anticyclone anomaly) in June located in the WNP, which enhanced the WNPSH substantially. However, the trend shifted northward from WNP to Japan and extratropical northern Pacific in July. The trend of Z850 did not contribute to the enhancement of WNPSH as it did in June. Consequently, the low-level wind in south China revealed a southwesterly (northeasterly) trend in June (July), which was in phase (against) the southwesterly monsoon flow.

In the present study, the effect of the warming trend includes all SSTs in various basins. Observation revealed that the IO and tropical western Pacific revealed the fast-warming trend in recent decades. Further numerical experiments are needed to force the model with SST warming in various regions to specify the individual effect.

Acknowledgments. This study was supported by the National Science and Technology Council (NSTC), Taiwan, under Grants 109-2111-M-845-001, 109-2123-M-001-004, 111-2111-M-845-001, and 112-2111-M-845-002.

Data availability statement. The GPCP v2.3 precipitation data and the ERSST v5 data were provided by NOAA/OAR/ESRL PSL, Boulder, Colorado, from their websites at https://psl.noaa.gov/data/gridded/data.gpcp.html and https://psl.noaa.gov/data/gridded/data.noaa.ersst.v5.html, respectively. The satellite-based datasets of CMORPH and PERSIAN were from https://doi.org/10.25921/w9va-q159 and https://chrsdata.eng.uci.edu, respectively. The ERA5 reanalysis data were obtained from Copernicus Climate Change Service (C3S) Climate Data Store (CDS) and are available at https://cds.climate.copernicus.eu/cdsapp#!/dataset/reanalysis-era5-pressure-levels-monthly-means?tab=form. The CMIP6 dataset was from https://esgf-node.llnl.gov/projects/cmip6. All calculation and figures were produced using the MATLAB and Statistics Toolbox Release 2021b version 9.11.0.1769968, the M_MAP mapping package for MATLAB version 1.4m (https://www.eoas.ubc.ca/~rich/map.html), and the NCAR Command Language (NCL) (https://www.ncl.ucar.edu/) version 6.3.0.

REFERENCES

Adler, R. F., and Coauthors, 2018: The Global Precipitation Climatology Project (GPCP) monthly analysis (new version 2.3) and a review of 2017 global precipitation. *Atmosphere*, **9**, 138, https://doi.org/10.3390/atmos9040138.

Ashouri, H., K.-L. Hsu, S. Sorooshian, D. K. Braithwaite, K. R. Knapp, L. D. Cecil, B. R. Nelson, and O. P. Prat, 2015: PERSIANN-CDR: Daily precipitation climate data record from multisatellite observations for hydrological and climate studies. *Bull. Amer. Meteor. Soc.*, **96**, 69–83, https://doi.org/10.1175/BAMS-D-13-00068.1.

Chang, C.-P., Y. Zhang, and T. Li, 2000a: Interannual and interdecadal variations of the East Asian summer monsoon and tropical Pacific SSTs. Part I: Roles of the subtropical ridge. *J. Climate*, **13**, 4310–4325, https://doi.org/10.1175/1520-0442(2000)013<4310:IAIVOT>2.0.CO;2.

——, ——, and ——, 2000b: Interannual and interdecadal variations of the East Asian summer monsoon and tropical Pacific SSTs. Part II: Meridional structure of the monsoon. *J. Climate*, **13**, 4326–4340, https://doi.org/10.1175/1520-0442(2000)013<4326:IAIVOT>2.0.CO;2.

Chang, T.-C., H.-H. Hsu, and C.-C. Hong, 2016: Enhanced influences of tropical Atlantic SST on WNP–NIO atmosphere–ocean coupling since the early 1980s. *J. Climate*, **29**, 6509–6525, https://doi.org/10.1175/JCLI-D-15-0807.1.

Ding, Y., Z. Wang, and Y. Sun, 2008: Inter-decadal variation of the summer precipitation in East China and its association with decreasing Asian summer monsoon. Part I: Observed evidences. *Int. J. Climatol.*, **28**, 1139–1161, https://doi.org/10.1002/joc.1615.

——, P. Liang, Y. Liu, and Y. Zhang, 2020: Multiscale variability of Meiyu and its prediction: A new review. *J. Geophys. Res. Atmos.*, **125**, e2019JD031496, https://doi.org/10.1029/2019JD031496.

——, Y. Liu, and Z.-Z. Hu, 2021: The record-breaking mei-yu in 2020 and associated atmospheric circulation and tropical SST anomalies. *Adv. Atmos. Sci.*, **38**, 1980–1993, https://doi.org/10.1007/s00376-021-0361-2.

Hersbach, H., and Coauthors, 2020: The ERA5 global reanalysis. *Quart. J. Roy. Meteor. Soc.*, **146**, 1999–2049, https://doi.org/10.1002/qj.3803.

Hong, C.-C., T.-C. Chang, and H.-H. Hsu, 2014: Enhanced relationship between the tropical Atlantic SST and the summertime western North Pacific subtropical high after the early 1980s. *J. Geophys. Res. Atmos.*, **119**, 3715–3722, https://doi.org/10.1002/2013JD021394.

——, M.-Y. Lee, H.-H. Hsu, N.-H. Lin, and B.-J. Tsuang, 2015: Tropical SST forcing on the anomalous WNP subtropical high during July–August 2010 and the record-high SST in the tropical Atlantic. *Climate Dyn.*, **45**, 633–650, https://doi.org/10.1007/s00382-014-2275-5.

——, W.-L. Tseng, H.-H. Hsu, M.-Y. Lee, and C.-C. Chang, 2021: Relative contribution of trend and interannually varying SST anomalies to the 2018 heat waves in the extratropical Northern Hemisphere. *J. Climate*, **34**, 6319–6333, https://doi.org/10.1175/JCLI-D-20-0556.1.

Huang, B., and Coauthors, 2017: Extended Reconstructed Sea Surface Temperature, version 5 (ERSSTv5): Upgrades, validations, and intercomparisons. *J. Climate*, **30**, 8179–8205, https://doi.org/10.1175/JCLI-D-16-0836.1.

Huffman, G. J., R. F. Adler, M. M. Morrissey, D. T. Bolvin, S. Curtis, R. Joyce, B. McGavock, and J. Susskind, 2001: Global Precipitation at one-degree daily resolution from multisatellite observations. *J. Hydrometeor.*, **2**, 36–50, https://doi.org/10.1175/1525-7541(2001)002<0036:GPAODD>2.0.CO;2.

Klein, S. A., B. J. Soden, and N.-C. Lau, 1999: Remote sea surface temperature variations during ENSO: Evidence for a tropical atmospheric bridge. *J. Climate*, **12**, 917–932, https://doi.org/10.1175/1520-0442(1999)012<0917:RSSTVD>2.0.CO;2.

Kosaka, Y., and H. Nakamura, 2006: Structure and dynamics of the summertime Pacific–Japan teleconnection pattern. *Quart. J. Roy. Meteor. Soc.*, **132**, 2009–2030, https://doi.org/10.1256/qj.05.204.

Kusunoki, S., R. Mizuta, and M. Matsueda, 2011: Future changes in the East Asian rain band projected by global atmospheric models with 20-km and 60-km grid size. *Climate Dyn.*, **37**, 2481–2493, https://doi.org/10.1007/s00382-011-1000-x.

Lau, N.-C., and M. J. Nath, 2003: Atmosphere–ocean variations in the Indo-Pacific sector during ENSO episodes. *J. Climate*, **16**, 3–20, https://doi.org/10.1175/1520-0442(2003)016<0003:AOVITI>2.0.CO;2.

Lee, W.-L., and Coauthors, 2020: Taiwan Earth System Model version 1: Description and evaluation of mean state. *Geosci. Model Dev.*, **13**, 3887–3904, https://doi.org/10.5194/gmd-13-3887-2020.

Liang, Y.-C., J.-Y. Yu, E. S. Saltzman, and F. Wang, 2017: Linking the tropical Northern Hemisphere pattern to the Pacific warm blob and Atlantic cold blob. *J. Climate*, **30**, 9041–9057, https://doi.org/10.1175/JCLI-D-17-0149.1.

Liu, B., Y. Yan, C. Zhu, S. Ma, and J. Li, 2020: Record-breaking Meiyu rainfall around the Yangtze River in 2020 regulated by the subseasonal phase transition of the North Atlantic Oscillation. *Geophys. Res. Lett.*, **47**, e2020GL090342, https://doi.org/10.1029/2020GL090342.

Lu, R., 2001: Interannual variability of the summertime North Pacific subtropical high and its relation to atmospheric convection over the warm pool. *J. Meteor. Soc. Japan*, **79**, 771–783, https://doi.org/10.2151/jmsj.79.771.

Nitta, T., 1987: Convective activities in the tropical western Pacific and their impact on the Northern Hemisphere summer circulation. *J. Meteor. Soc. Japan*, **65**, 373–390, https://doi.org/10.2151/jmsj1965.65.3_373.

Qian, W., and D.-K. Lee, 2000: Seasonal march of Asian summer monsoon. *Int. J. Climatol.*, **20**, 1371–1386, https://doi.org/10.1002/1097-0088(200009)20:11<1371::AID-JOC538>3.0.CO;2-V.

Song, Z., C. Zhu, J. Su, and B. Liu, 2016: Coupling modes of climatological intraseasonal oscillation in the East Asian summer monsoon. *J. Climate*, **29**, 6363–6382, https://doi.org/10.1175/JCLI-D-15-0794.1.

Student, 1908: The probable error of a mean. *Biometrika*, **6** (1), 1–25, https://doi.org/10.2307/2331554.

Stuecker, M. F., F.-F. Jin, A. Timmermann, and S. McGregor, 2015: Combination mode dynamics of the anomalous northwest Pacific anticyclone. *J. Climate*, **28**, 1093–1111, https://doi.org/10.1175/JCLI-D-14-00225.1.

Sui, C.-H., P.-H. Chung, and T. Li, 2007: Interannual and interdecadal variability of the summertime western North Pacific subtropical high. *Geophys. Res. Lett.*, **34**, L11701, https://doi.org/10.1029/2006GL029204.

Takaya, Y., I. Ishikawa, C. Kobayashi, H. Endo, and T. Ose, 2020: Enhanced Meiyu-Baiu rainfall in early summer 2020: Aftermath of the 2019 super IOD event. *Geophys. Res. Lett.*, **47**, e2020GL090671, https://doi.org/10.1029/2020GL090671.

Tao, S. Y., and L. X. Chen, 1987: A review of recent research of the East Asian summer monsoon in China. *Monsoon Meteorology*, C.-P. Chang and T. N. Krishnamurti, Eds., Oxford University Press, 60–92.

Wang, B., and LinHo, 2002: Rainy season of the Asian–Pacific summer monsoon. *J. Climate*, **15**, 386–398, https://doi.org/10.1175/1520-0442(2002)015<0386:RSOTAP>2.0.CO;2.

——, R. Wu, and X. Fu, 2000: Pacific–East Asian teleconnection: How does ENSO affect East Asian climate? *J. Climate*, **13**, 1517–1536, https://doi.org/10.1175/1520-0442(2000)013<1517:PEATHD>2.0.CO;2.

——, Z. Wu, J. Li, J. Liu, C.-P. Chang, Y. Ding, and G. Wu, 2008: How to measure the strength of the East Asian summer monsoon. *J. Climate*, **21**, 4449–4463, https://doi.org/10.1175/2008JCLI2183.1.

Wang, Y.-C., and Coauthors, 2021: Performance of the Taiwan Earth System Model in simulating climate variability compared with observations and CMIP6 model simulations. *J. Adv. Model. Earth Syst.*, **13**, e2020MS002353, https://doi.org/10.1029/2020MS002353.

Webster, P. J., A. M. Moore, J. P. Loschnigg, and R. R. Leben, 1999: Coupled ocean–atmosphere dynamics in the Indian Ocean during 1997–98. *Nature*, **401**, 356–360, https://doi.org/10.1038/43848.

Wei, K., C. Ouyang, H. Duan, Y. Li, M. Chen, J. Ma, H. An, and S. Zhou, 2020: Reflections on the catastrophic 2020 Yangtze River Basin flooding in southern China. *Innovation*, **1**, 100038, https://doi.org/10.1016/j.xinn.2020.100038.

Weller, E., S.-K. Min, W. Cai, F. W. Zwiers, Y.-H. Kim, and D. Lee, 2016: Human-caused Indo-Pacific warm pool expansion. *Sci. Adv.*, **2**, e1501719, https://doi.org/10.1126/sciadv.1501719.

Weng, H., K.-M. Lau, and Y. Xue, 1999: Multi-scale summer rainfall variability over China and its long-term link to global sea surface temperature variability. *J. Meteor. Soc. Japan*, **77**, 845–857, https://doi.org/10.2151/jmsj1965.77.4_845.

Wu, B., T. Li, and T. Zhou, 2010: Relative contributions of the Indian Ocean and local SST anomalies to the maintenance of the western North Pacific anomalous anticyclone during the El Niño decaying summer. *J. Climate*, **23**, 2974–2986, https://doi.org/10.1175/2010JCLI3300.1.

Wu, R., and B. Wang, 2000: Interannual variability of summer monsoon onset over the western North Pacific and the underlying processes. *J. Climate*, **13**, 2483–2501, https://doi.org/10.1175/1520-0442(2000)013<2483:IVOSMO>2.0.CO;2.

Wu, T., A. Hu, F. Gao, J. Zhang, and G. A. Meehl, 2019: New insights into natural variability and anthropogenic forcing of global/regional climate evolution. *npj Climate Atmos. Sci.*, **2**, 18, https://doi.org/10.1038/s41612-019-0075-7.

Wu, Y.-K., A.-Y. Huang, C.-K. Wu, C.-C. Hong, and C.-C. Chang, 2020: Effect of warm SST in the subtropical eastern North Pacific on triggering the abrupt change of the mei-yu rainfall over South China in the early 1990s. *J. Climate*, **33**, 657–673, https://doi.org/10.1175/JCLI-D-18-0292.1.

Xie, P., R. Joyce, S. Wu, S.-H. Yoo, Y. Yarosh, F. Sun, and R. Lin, 2017: Reprocessed, bias-corrected CMORPH global high-resolution precipitation estimates from 1998. *J. Hydrometeor.*, **18**, 1617–1641, https://doi.org/10.1175/JHM-D-16-0168.1.

Xie, S.-P., K. Hu, J. Hafner, H. Tokinaga, Y. Du, G. Huang, and T. Sampe, 2009: Indian Ocean capacitor effect on Indo–western Pacific climate during the summer following El Niño. *J. Climate*, **22**, 730–747, https://doi.org/10.1175/2008JCLI2544.1.

Yang, J., Q. Liu, S.-P. Xie, Z. Liu, and L. Wu, 2007: Impact of the Indian Ocean SST basin mode on the Asian summer monsoon. *Geophys. Res. Lett.*, **34**, L02708, https://doi.org/10.1029/2006GL028571.

Zhang, W., Z. Huang, F. Jiang, M. F. Stuecker, G. Chen, and F.-F. Jin, 2021: Exceptionally persistent Madden-Julian Oscillation activity contributes to the extreme 2020 East Asian summer monsoon rainfall. *Geophys. Res. Lett.*, **48**, e2020GL091588, https://doi.org/10.1029/2020GL091588.

Zhao, N., A. Manda, X. Guo, K. Kikuchi, T. Nasuno, M. Nakano, Y. Zhang, and B. Wang, 2021. A Lagrangian view of moisture transport related to the heavy rainfall of July 2020 in Japan: Importance of the moistening over the subtropical regions. *Geophys. Res. Lett.*, **48**, e2020GL091441, https://doi.org/10.1029/2020GL091441.

Zheng, J., and C. Wang, 2021: Influences of three oceans on record-breaking rainfall over the Yangtze River Valley in June 2020. *Sci. China Earth Sci.*, **64**, 1607–1618, https://doi.org/10.1007/s11430-020-9758-9.

Zhou, Z.-Q., S.-P. Xie, and R. Zhang, 2021: Historic Yangtze flooding of 2020 tied to extreme Indian Ocean conditions. *Proc. Natl. Acad. Sci. USA*, **118**, e2022255118, https://doi.org/10.1073/pnas.2022255118.